Mecánica Computacional Vol. XXIII, pp. 2301-2318
G.Buscaglia, E.Dari, O.Zamonsky (Eds.)
Bariloche, Argentina, November 2004

3D-THERMO-MECHANICAL SIMULATION OF WELDING PROCESSES

A. Anca*, A. Cardona, and J.M. Risso

Centro Internacional de Métodos Computacionales en Ingeniería (CIMEC)
Universidad Nacional del Litoral–CONICET
Güemes 3450, 3000, Santa Fe, Argentine
*e-mail: aanca@intec.unl.edu.ar

Key Words: Residual Stresses, Welding Simulation, Non-isothermal Phase Change.

Abstract.

This paper presents a numerical approach for 3D simulation of welding processes. The main objective of this simulation is the determination of temperatures and stresses during and after the process. Temperature distribution define the heat affected zone where material properties are affected. Stress calculation is necessary because high residual stresses may promote brittle fractures, fatigue, or stress corrosion in regions near the weld. The finite element method has been used to perform 1) a thermal analysis involving non-isothermal phase change and 2) a mechanical elasto-plastic analysis. Comparisons between analytical and numerical results for a non-isothermal solidification test case are presented.

1 INTRODUCTION

Welding is defined by the American Welding Society (AWS) as a localized coalescence of metals or non-metals produced by either heating of the materials to a suitable temperature with or without the application of pressure, or by the application of pressure alone, with or without the use of filler metal.[1]

There are various welding processes used in industry today, the main factors for their distinctions being the source of the energy used for welding, and the means of protection or cleaning of the welded material. In this paper we are concerned on welding methods that only involve heating of metals.

Information about the shape, dimensions and residual stresses in a component after welding are of great interest in order to improve quality and to prevent failures during manufacturing or in service. Information about the residual stresses also gives input for lifetime prediction, which is important in the industry. Process parameters and different fixture set-ups can be evaluated without doing a large number of experiments by the use of a virtual model. This problem and many others directly associated with it, have been studied by several researchers.[1,2]

Different physical phenomena occur during the welding process, involving the interaction of thermal, mechanical, electrical and metallurgical phenomena.[3] The temperature field is a function of many welding parameters such as arc power, welding speed, welding sequences and environmental conditions.[4] Formation of distortions and residual stresses in weldments depends on many interrelated factors such as thermal field, material properties, structural boundary conditions, types of welding operation and welding conditions.

From a mechanical viewpoint, distortions and residual stresses induced in structures after welding can be regarded as the resultant of incompatible strains consisting of plastic strains, creep strains, and others. In this study, it is assumed that only plastic strains exist as the incompatible strains after welding, because creep would not be expected due to fast cooling, and no thermal strains are expected after completion of cooling.[5]

Simulation of continuous welding seams can be done by means of nonlinear and non-stationary thermal, metallurgical and mechanical analysis. The transient behavior during welding is not possible to predict in a 2D model because it corresponds to infinite welding speed in the thermal analysis. Moreover, the use of three-dimensional thermal models, which have the ability to simulate the effect of arc movement, is recommended for both multi-layer and multi-block welding.[4] Due to these reasons, the current work was focused on three-dimensional study of thermal and mechanical processes during welding.

A multi-dimensional solidification problem in which solidification takes place over a temperature range (typical in steel alloys) is implemented following a discontinuous integration scheme[6] along the discontinuities that involves this kind of problem.

We extend the previous work of Fachinotti et al.[7,8] about coupled thermo-mechanical models applied to continuous casting simulations, developing a 3D transient thermo-mechanical model using a Lagrangian formulation. The material model used in this paper is a rate independent isotropic plasticity model[9] that does not account for microstructure variations and does not

include effects of transformation induced plasticity (TRIP). These effects will be included in the future.

The paper is organized as follows. In Section 2 and 3, we describe the developed model for the thermal and mechanical problems, their hypotheses and the equations involved and also the discretization procedure to obtain the set of equations in both fields. Section 4 describes briefly the strategy used to solve the coupled thermo-mechanical problem.

2 THERMAL PROBLEM

2.1 Introduction

In this section a temperature-based model to simulate the unsteady conduction heat transfer problem in a 3D media undergoing mushy phase change is described.

It is a extension of the method previously formulated for solving 2D and axisymmetric transient conduction[10] and steady state conduction-advection phase-change problems.[11]

The analyzed domain is discretized using linear tetrahedral finite elements. Galerkin weighting functions are used.

During phase change, a considerable amount of latent heat is released or absorbed, causing a strong non-linearity in the enthalpy function. In order to model correctly such phenomenon, we distinguish the different one-phase subregions encountered when integrating over those finite elements embedded into the solidification front.

Contributions from different phases are integrated separately in order to capture the sharp variations of the material properties between phases. This so called discontinuous integration avoids the regularization of the phenomenon, allowing the exact evaluation of the discrete non-linear governing equation, which are solved using a full Newton-Raphson scheme, together with line-search.

We validate the performance of the thermal model by comparison with an exact solution.[12]

2.2 Problem definition

Under the assumptions of incompressibility, negligible viscosity and dissipation, linear dependence of the heat flux on temperature gradient (Fourier's law), and no melt flow during the solidification process the energy balance for each subdomain Ω_i is governed by the equations

$$\rho \frac{\partial \mathcal{H}}{\partial t} - \nabla \cdot (\kappa \nabla T) = 0 \quad \forall (\boldsymbol{x}, t) \in \Omega_i \tag{1}$$

where T denotes the temperature, $\mathcal{H}$ the enthalpy (per unit volume) and $\kappa = \kappa(T)$ the material thermal conductivity, assumed isotropic. Equation (1) is supplemented by the following initial condition

$$T = T_0 \quad \forall \boldsymbol{x} \in \Omega_i, \quad t = t_0$$

and external boundary conditions at $\partial\Omega$:

$$T = \bar{T} \quad \text{at } \partial\Omega_T \tag{2}$$
$$-\kappa\nabla T \cdot \boldsymbol{n} = \bar{q} \quad \text{at } \partial\Omega_q \tag{3}$$
$$-\kappa\nabla T \cdot \boldsymbol{n} = h_{env}(T - T_{env}) \quad \text{at } \partial\Omega_c \tag{4}$$

being $\partial\Omega_T$, $\partial\Omega_q$ and $\partial\Omega_c$ non-overlapping portions of $\partial\Omega$, with prescribed temperature, conductive and convective heat flux, respectively. In the above, $\bar{T}$ and $\bar{q}$ refer to imposed temperature and heat flux fields, and T_{env} is the temperature of the environment, whose film coefficient is h_{env}; $\boldsymbol{n}$ denotes the unit outward normal to $\partial\Omega$.

Further, the following boundary conditions must hold at the interface(s) Γ:

$$T = T_\Gamma \tag{5}$$
$$\langle \mathcal{H}u(\boldsymbol{\eta}) + \kappa\nabla T \cdot \boldsymbol{\eta} \rangle = 0 \tag{6}$$

where T_Γ is a constant value (equal to the melting temperature for isothermal solidification, and either the solidus or liquidus temperature otherwise), $\langle * \rangle$ denotes the jump of the quantity $(*)$ in crossing the interface Γ, which is moving with speed u in the direction given by the unit vector $\boldsymbol{\eta}$. Note that the second equation states the jump energy balance at the interface.

In order to retrieve T as the only primal variable, we define the enthalpy as

$$\mathcal{H}(T) = \int_{T_{ref}}^{T} \rho c \mathrm{d}\tau + \rho\mathcal{L} f_l \tag{7}$$

being ρc and $\rho\mathcal{L}$ the unit volume heat capacity and latent heat, respectively, and T_{ref} an arbitrary reference temperature; f_l is a characteristic function of temperature, called volumetric liquid fraction, defined as

$$f_l(T) = \begin{cases} 0 & \text{if } T < T_{sol} \\ 0 \leq f_l^m(T) \leq 1 & \text{if } T_{sol} \leq T \leq T_{liq} \\ 1 & \text{if } T > T_{liq} \end{cases} \tag{8}$$

where T_{sol} and T_{liq} denote the solidus and liquidus temperatures, respectively, i.e., the lower and upper bounds of the mushy temperature range.

2.3 Finite element formulation

First, we derive the weak or variational form of the balance equation (1), supplied by the boundary conditions (2-6), using the weighted residual method. The proper choice of weighting functions together with the application of Reynolds' transport theorem allow to cancel the terms arising from the interface conditions (6). And using the definition in (7) then we have the weak temperature-based form of the governing equation:

$$\int_\Omega W\rho c\frac{\partial T}{\partial t}\,\mathrm{d}V + \frac{\partial}{\partial t}\int_\Omega W\rho\mathcal{L}f_l\,\mathrm{d}V + \int_\Omega \kappa\nabla W\cdot\nabla T\,\mathrm{d}V + \int_{\partial\Omega_q} W\bar{q}\,\mathrm{d}S + \\ + \int_{\partial\Omega_c} Wh_{env}(T-T_{env})\,\mathrm{d}S = 0 \tag{9}$$

where W is the weighting function.

In the finite element context, the unknown field T approximates to a linear combination of interpolation functions $N_i(x,y,z)$, the so-called shape functions, as follows:

$$T(x,y,z) = \sum_i^N N_i(x,y,z)T_i \tag{10}$$

being T_i the temperature at each node i $(i = 1, 2, \cdots, N)$ arising from the discretization of the analyzed domain Ω.

After substituting T by its approximation (10) into equation (9), we have to define the weighting function W. Adopting $W \equiv N_i$ (Galerkin method), we get a non linear system of N ordinary differential equations, stated in matrix form as

$$\boldsymbol{\Psi} = \boldsymbol{C}\frac{\partial \boldsymbol{T}}{\partial t} + \frac{\partial \boldsymbol{L}}{\partial t} + \boldsymbol{K}\boldsymbol{T} - \boldsymbol{F} = 0 \tag{11}$$

where $\boldsymbol{T}$ is the vector of unknown nodal temperatures, $\boldsymbol{C}$ the capacity matrix, $\boldsymbol{L}$ the latent heat vector, $\boldsymbol{K}$ the conductivity (stiffness) matrix and $\boldsymbol{F}$ the force vector.

Each term of the residual vector $\boldsymbol{\Psi}$ are given (in components) by:

$$\begin{aligned} C_{ij} &= \int_\Omega \rho c\, N_i N_j\,\mathrm{d}V \\ L_i &= \int_\Omega \rho\mathcal{L}f_l N_i\,\mathrm{d}V \\ K_{ij} &= \int_\Omega \kappa\nabla N_i\cdot\nabla N_j\,\mathrm{d}V + \int_{\partial\Omega_c} h_{env}\,N_i N_j\,\mathrm{d}S. \end{aligned} \tag{12}$$

On the other hand, the load vector $\boldsymbol{F}$ takes the form:

$$F_i = -\int_{\partial\Omega_q} \bar{q}N_i\,\mathrm{d}S + \int_{\partial\Omega_c} h_{env}T_{env}N_i\,\mathrm{d}S. \tag{13}$$

2.4 Discontinuous integration in linear tetrahedral elements

As we are following the same integration scheme as in[10,11] we describe now briefly the discontinuous integration of a linear tetrahedra. In a linear tetrahedral element the interfaces

(isotherms) are planes inside each element. Therefore, the different one-phase subregions encountered in an element affected by phase change always show polyhedral geometries. This fact allows to solve exactly the integrals (14) in a relatively easy manner.

The use of linear elements produces an element-wise constant approximation to the temperature gradient, $\nabla N_i T_i$.

The plain transient conduction problem in the absence of phase change has been widely discussed in the classic finite element literature (see e.g. Zienkiewicz and Taylor[13]). Then ,we shall focus on the latent heat effects, as given in general form by equation (12). Let us consider the contribution of a typical linear tetrahedral element e to $\boldsymbol{L}$ that involves phase change:

$$L_i^e = \rho\mathcal{L} \int_{\Omega_l^e} N_i^e \, \mathrm{d}V \; + \rho\mathcal{L} \int_{\Omega_m^e} f_l N_i^e \, \mathrm{d}V \tag{14}$$

the above integrals extend over the element liquid Ω_l^e and mushy Ω_m^e subdomains

We assume that the latent heat is uniformly released or absorbed during solidification such that f_l comes out a linear function of T,

$$f_l = \frac{T - T_{sol}}{T_{liq} - T_{sol}}. \tag{15}$$

Looking at the simplicity of the above expressions, the advantage of choosing a linear tetrahedral finite element is noticeable. In fact, computation of the volume V_m^e (and its center) is trivial when it is tetrahedral, i.e., for the fully-mushy element and cases $sssm$ and $mlll$ in Figure 1. Also, it can be expressed as the difference between tetrahedral volumes in cases $smmm$, $mmml$, $sssl$, $slll$ and $smml$. For pentahedral mushy volumes not embodied in the previous classification, i.e. cases $ssmm$ and $mmll$, we assume Ω_m^e split into three tetrahedra (see Figure 2). Finally, we can evaluate the remainder (hexahedral) mushy configurations ($ssll$, $ssml$ and $smll$) as differences between tetrahedra and pentahedra.

Remark: We can accurately approximate any non-linear liquid fraction f_l using a piecewise linear function f_l^*. Let f_l be equal to f_l^* at a series of abscissa $T_0 = T_{sol} < T_1 < \cdots < T_n = T_{liq}$. Now we can think of $\boldsymbol{L}$ as the summation of contributions arising from n partial mushy zones, each one defined by a temperature range $[T_{i-1}, T_i]$ ($i = 1, 2, \cdots, n$) within which a portion $\rho\mathcal{L}_i = \rho\mathcal{L}[f_l(T_i) - f_l(T_{i-1})]$ is uniformly released or absorbed.

2.5 Solution scheme

Time integration in transient problems is done with the unconditionally stable first-order backward Euler method . This implicit scheme is applied on equation (11), which leads to a set of non-linear equations to be solved for the values of the temperatures at finite element nodes, at the end of the time increment considered:

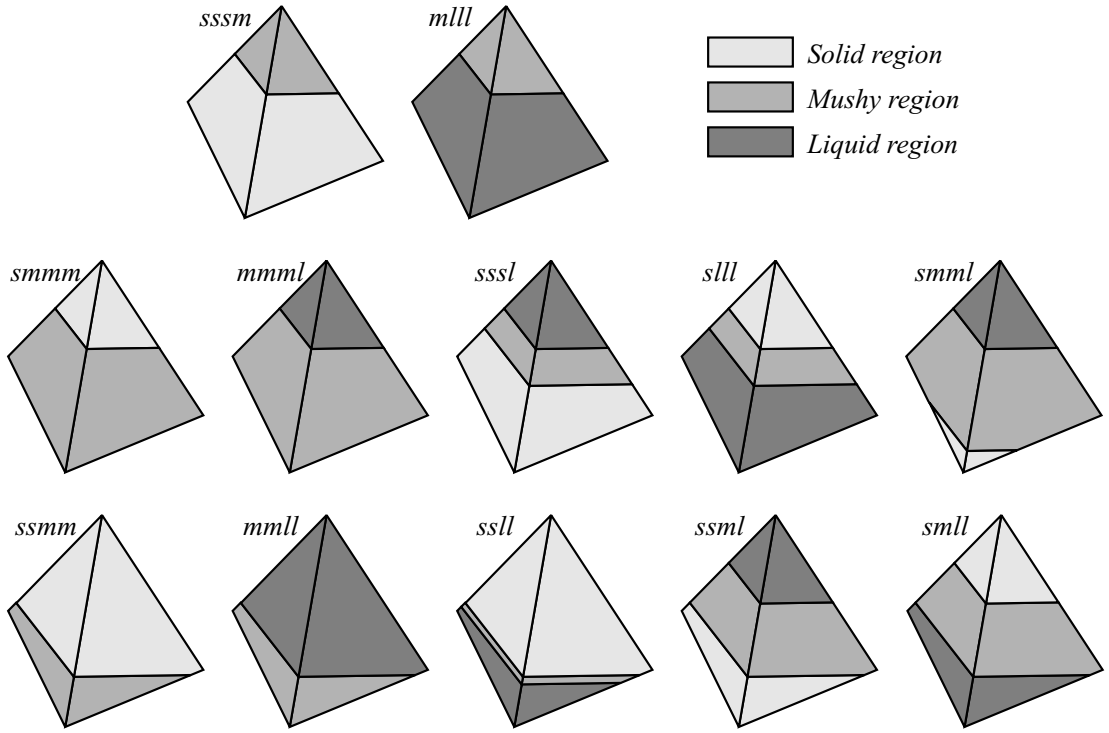

Figure 1: Different configurations of linear tetrahedral finite elements affected by mushy phase change.

$$\boldsymbol{\Psi}_{n+1} = \boldsymbol{C}_{n+1}\frac{\boldsymbol{T}_{n+1}-\boldsymbol{T}_n}{\Delta t} + \frac{\boldsymbol{L}_{n+1}-\boldsymbol{L}_n}{\Delta t} + \boldsymbol{K}_{n+1}\boldsymbol{T}_{n+1} - \boldsymbol{F}_{n+1} = \boldsymbol{0} \tag{16}$$

The solution of the highly non-linear discrete balance equation (16) is achieved by means of the well-known Newton-Raphson method. Because of its quadratic convergence rate, it provides probably the fastest way to solve non-linear equations,[13] whenever the initial solution lays within the convergence or "attraction" zone.

At each new iteration i, $\boldsymbol{\Psi}$ is approximated using a first order Taylor expansion,

$$\boldsymbol{\Psi}_{(\boldsymbol{T}^{(i)})} \approx \boldsymbol{\Psi}_{(\boldsymbol{T}^{(i-1)})} + \boldsymbol{J}_{(\boldsymbol{T}^{(i-1)})}\Delta\boldsymbol{T}^{(i)} = \boldsymbol{0} \tag{17}$$

being $\boldsymbol{J} = \mathrm{d}\boldsymbol{\Psi}/\mathrm{d}\boldsymbol{T}$ the Jacobian or tangent matrix, and $\Delta\boldsymbol{T}^{(i)} = \boldsymbol{T}^{(i)} - \boldsymbol{T}^{(i-1)}$, the search direction. Iterative correction of temperatures is defined by:

$$\Delta\boldsymbol{T}^{(i)} = -[\boldsymbol{J}_{(\boldsymbol{T}^{(i-1)})}]^{-1}\boldsymbol{\Psi}_{(\boldsymbol{T}^{(i-1)})} \tag{18}$$

All the terms of the tangent matrix for transient conduction heat transfer, may be found in the classical texts, e.g. Zienkiewicz and Taylor;[13] but the latent heat contribution $\frac{\mathrm{d}\boldsymbol{L}}{\mathrm{d}\boldsymbol{T}}$ is detailed below. This particular matrix is the assemblage of the elemental matrices:

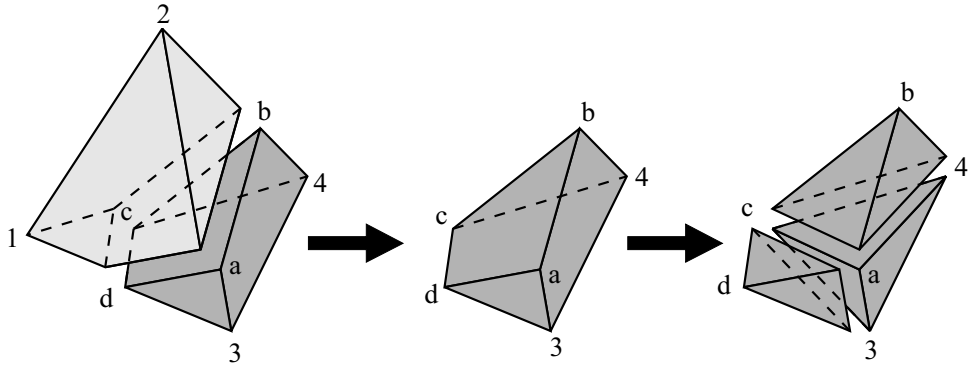

Figure 2: Split of a pentahedral mushy region into three tetrahedra.

$$\frac{\mathrm{d}\boldsymbol{L}^e}{\mathrm{d}\boldsymbol{T}^e} = \boldsymbol{C}_L^e + \frac{\mathrm{d}\boldsymbol{C}_L^e}{\mathrm{d}\boldsymbol{T}^e}\boldsymbol{T}^e - \frac{\rho\mathcal{L}T_{sol}}{T_{liq}-T_{sol}}\left[\frac{\mathrm{d}\boldsymbol{N}^e(\boldsymbol{x}_{bar,m})}{\mathrm{d}\boldsymbol{T}^e}V_m^e + \boldsymbol{N}^e(\boldsymbol{x}_{bar,m})\frac{\mathrm{d}V_m^e}{\mathrm{d}\boldsymbol{T}^e}\right] + \\ +\rho\mathcal{L}\left[\frac{\mathrm{d}\boldsymbol{N}^e(\boldsymbol{x}_{bar,l})}{\mathrm{d}\boldsymbol{T}^e}V_l^e + \boldsymbol{N}^e(\boldsymbol{x}_{bar,l})\frac{\mathrm{d}V_l^e}{\mathrm{d}\boldsymbol{T}^e}\right] \tag{19}$$

where

$$\boldsymbol{C}_L^e = \frac{\rho\mathcal{L}}{T_{liq}-T_{sol}}\int_{\Omega_m^e}\boldsymbol{N}^e\boldsymbol{N}^{e^T}\,\mathrm{d}V \tag{20}$$

being V_l^e, V_m^e the volumes of liquid and mushy zones and $\boldsymbol{x}_{bar,l}$, $\boldsymbol{x}_{bar,m}$ the barycenter of the liquid and mushy subregions respectively.

As aforementioned, Newton-Raphson is efficient provided that the initial guess $\boldsymbol{T}^{(0)}$ lies within the convergence radius of the solution $\boldsymbol{T}$. If it is not the case, convergence can be forced using a line-search procedure.[14] Assuming that $\Delta\boldsymbol{T}$ as defined by equation (18) is the correct search direction, we predict $\boldsymbol{T}$ at the iteration i as follows

$$\boldsymbol{T}^{(i)} = \boldsymbol{T}^{(i-1)} + \beta\Delta\boldsymbol{T}^{(i)} \tag{21}$$

being the scalar parameter β determined under the condition of orthogonality between the new residual vector and the search direction, i.e.,

$$\boldsymbol{\Psi}(\boldsymbol{T}^{(i)})\cdot\Delta\boldsymbol{T}^{(i)} = 0. \tag{22}$$

Line-search must be activated whenever

$$\boldsymbol{\Psi}(\boldsymbol{T}^{(i-1)} + \Delta\boldsymbol{T}^{(i)})\cdot\Delta\boldsymbol{T}^{(i)} > k\boldsymbol{\Psi}(\boldsymbol{T}^{(i)})\cdot\Delta\boldsymbol{T}^{(i)}. \tag{23}$$

For the application presented below, the factor k was chosen to be unit. Reference[10] contains a detailed description of the currently implemented algorithm.

2.6 Validation - A benchmark problem

Verification of the model has been performed comparing numerical and analytical results for a transient non-linear heat transfer problem with exact solution. This is a benchmark problem that is concerned with the solidification of a material which is initially at a temperature just above its freezing point and subject to a line heat sink in a infinite medium with cylindrical symmetry. The substance have an extended freezing temperature range between the solidus and liquidus temperatures. This problem was solved exactly by Özisik and Uzzel.[12] The solid fraction is assumed to vary linearly with the temperature. As the material has a high latent heat, severe numerical discontinuities are present at the liquid-solid boundary. The material properties are summarized in table 1. Only a circular sector of the cylinder, forming a wedge, was discretized because of the symmetry.

The cylinder surface at $r = L$ is maintained at a constant, uniform temperature T_i. The dimensions of the wedge are: radius = 1 m, sector angle = 15 degrees, and thickness = 0.01 m. The mesh is shown in figure 5.

Parameter	Symbol	Value	Unit
Density	ρ	2723.2	$[kg/m^3]$
Specific Heat, (solid)	C_s	1046.7	$[J/kg^oC]$
Specific Heat, (liquid)	C_l	1256.0	$[J/kg^oC]$
Latent Heat	$\mathcal{L}$	395403	$[J/kg]$
Conductivity (solid)	κ_s	197.3	$[W/m^oC]$
Conductivity (liquid)	κ_l	181.7	$[W/m^oC]$
Solidus temp.	T_s	547.8	$[^oC]$
Liquidus temp.	T_l	642.2	$[^oC]$
Initial temp.	T_i	648.9	$[^oC]$
Line heat sink	Q	50000	$[W/m]$

Table 1: *Material and problem data for the validation problem*

The numerical results are in agreement with the corresponding analytical results as shown in figure 3.

The use of a concentrated heat sink leads to large thermal gradients as $r \to 0$. This singularity explains the error increment in the vicinity of the axis (see fig.4).

As described in,[15] a concentrated thermal load in an infinite half space has a singularity proportional to the inverse of the radial distance. Therefore concentration of elements and nodes around the (welding) source where gradients change rapidly is required. In figure 4 the relative errors between the exact and 3D FEM solution is plotted.

Figure 5 offers a general view of the computed temperature distribution through the domain 1 hour after starting of tht process.

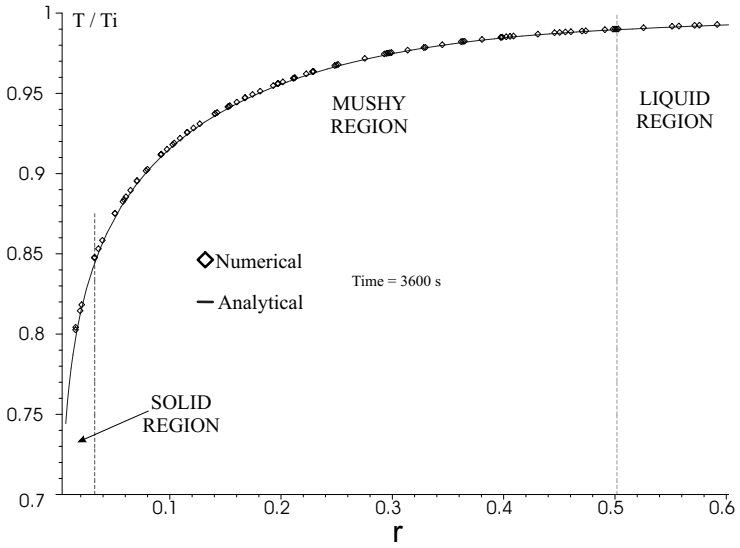

Figure 3: Temperature comparison: FEM vs. analytical solution

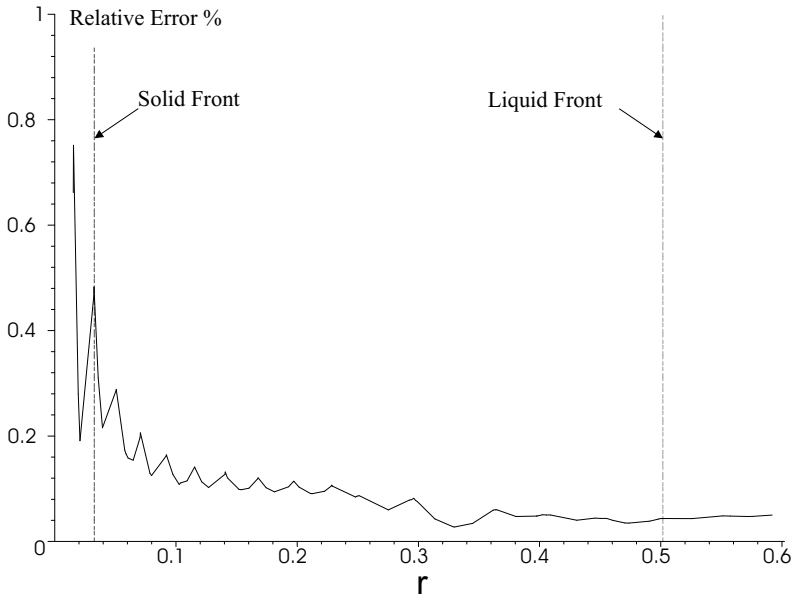

Figure 4: Relative error (%) between numeric and analytic solutions

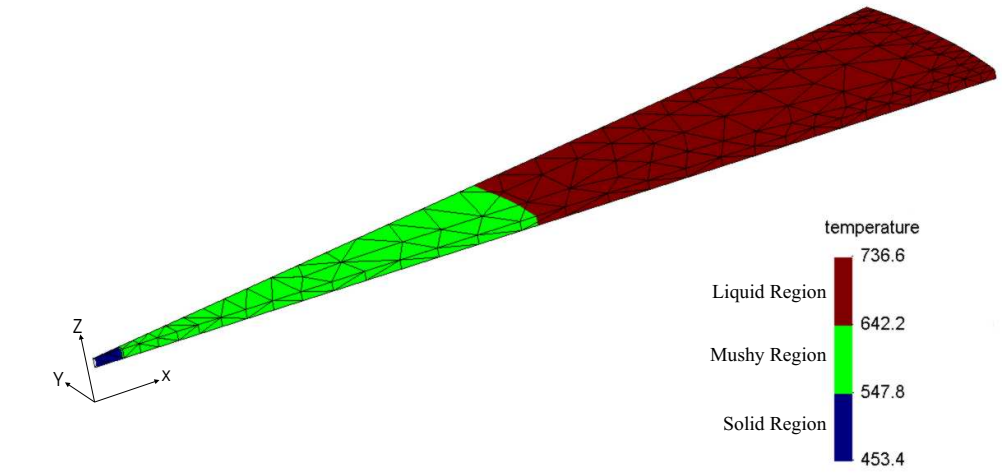

Figure 5: FEM mesh and temperature distribution at t=1 hour

3 MECHANICAL PROBLEM

3.1 Introduction

During a thermal welding process, the weld site and immediate surrounding area experience different rates of heating/cooling and thus expansion/contraction, that leads to considerable thermal strains. Due to the localized nature of the heat application, the expansion due to these strains is constrained by the cooler material away from the site of the applied heat. The physical and chemical properties of the material also change at the weld site and heat affected zone (HAZ), both during and after the welding process. These changes affect mechanical material properties, and must be taken into account in mechanical analysis.

Due to the intrinsic three-dimensional nature of loads, boundary conditions and geometry usually involved in welding processes, a 3D mechanical model was implemented. It should be noted that the weld pool itself is not modelled in mechanical analysis. This is only a soft region serving as the means of the heat input to the thermomechanical model. In this sense, the use of cut-off temperature or zero-strength temperature, ZST was assumed. This is also the temperature above which no further changes in material properties are accounted for in the mechanical analysis.

The thermoelastic material behavior is for most cases based on a hypoelastic version of Hooke's law with inclusions of thermal strains. The Young's modulus, and the thermal dilatation coefficient, are the most important parameters. Poisson ratio, has a smaller influence[16] on

the residual stresses and deformations. The plastic material model for solidified metal was the rate-independent, incompressible Von Mises plasticity. An associative flow rule was used and isotropic hardening have been assumed.

The argument for using rate-independent plasticity at high temperatures is based on the involved time scales.[17] The material has a high temperature during a relatively short time of the weld thermal cycle, and therefore the accumulated rate-dependent plasticity is neglected.

Inertial effects are ignored in momentum balance equations, according to the assumption of null velocity field within the solid.

3.2 Lagrangian formulation of the constitutive equations

According to the local state theory,[18] the thermodynamic state at any particle $\boldsymbol{X}$ of a material medium at a given instant t is completely defined by the values of a certain number of state variables at this particle, at this instant. Computations on inelastic materials take advantage of strain-driven formulations, in which state variables are the total strain $\boldsymbol{\varepsilon}$ and a set of phenomenological internal strain-type variables describing material history, together with the temperature field T, here assumed to be known a priori.

No kinematic nonlinearities are taken into account, or equivalently small strains and displacements are assumed.[19] Even when small strain approximations are often used in this type of problems, one must be aware that even moderate rotations will create spurious stresses.[20]

Then, the total strain can be additively decomposed as follows:

$$\boldsymbol{\varepsilon} = \boldsymbol{\varepsilon}^e + \boldsymbol{\varepsilon}^i, \tag{24}$$

$\boldsymbol{\varepsilon}^e$ being the thermoelastic (reversible) strain and $\boldsymbol{\varepsilon}^i$ the inelastic (irreversible) strain. Either term may play the role of an internal variable, but $\boldsymbol{\varepsilon}^i$ is typically chosen (option we followed in this work).

We also adopt a scalar internal variable α, which characterizes isotropic hardening from the phenomenological point of view. The hypothesis of isotropic hardening is widely accepted in welding applications.[17,21,22]

Furthermore, the most popular choice for the hardening parameter α relies on the equivalent inelastic strain:

$$\alpha = \int_0^t \sqrt{\frac{2}{3}}\, \|\dot{\boldsymbol{\varepsilon}}^i(\tau)\|\, \mathrm{d}\tau, \tag{25}$$

where $\dot{\boldsymbol{\varepsilon}}^i$ is the inelastic strain rate and $\|\dot{\boldsymbol{\varepsilon}}^i\| = \sqrt{\dot{\varepsilon}^i_{ij}\dot{\varepsilon}^i_{ij}}$ its L_2-norm.

Although driving variables lie in strain space, response functions (i.e. the yield criterion and the evolution laws) are usually written in terms of their conjugated thermodynamic forces: the stress tensor $\boldsymbol{\sigma}$ (dual of $\boldsymbol{\varepsilon}^e$) and the isotropic hardening variable in stress space, $R = R(\alpha)$.

The stress tensor $\boldsymbol{\sigma}$ depends on $\boldsymbol{\varepsilon}$ and $\boldsymbol{\varepsilon}^i$ through the decomposition (24). For linearly-elastic

isotropic materials, the stress is defined by the state law:

$$\boldsymbol{\sigma} = \underbrace{\kappa\,[\,\mathrm{tr}\,(\boldsymbol{\varepsilon}^e) - 3\varepsilon_T]}_{p}\,\boldsymbol{l} + \underbrace{2\mu\,\mathrm{dev}(\boldsymbol{\varepsilon}^e)}_{\boldsymbol{s}}, \tag{26}$$

where $\kappa = \kappa(T)$ and $\mu = \mu(T)$ are thermo-dependent material properties known as bulk and shear moduli, respectively, ε_T is the thermal strain, $\boldsymbol{l}$ the second-order unit tensor, $\mathrm{tr}\,(\boldsymbol{\varepsilon}^e) = \varepsilon^e_{ii}$ and $\mathrm{dev}(\boldsymbol{\varepsilon}^e) = \boldsymbol{\varepsilon}^e - \mathrm{tr}\,(\boldsymbol{\varepsilon}^e)\boldsymbol{l}/3$ are the trace and the deviator of the second-order tensor $\boldsymbol{\varepsilon}^e$, $p = \mathrm{tr}\,(\boldsymbol{\sigma})/3$ is the mean stress and $\boldsymbol{s} = \mathrm{dev}(\boldsymbol{\sigma})$ is the stress deviator. Here, the thermal expansion is defined by the thermal linear expansion (TLE) function:

$$\varepsilon_T = \mathrm{TLE}\,(T) = \int_{T_{ref}}^{T} \alpha_T(\tau)\,\mathrm{d}\tau, \tag{27}$$

with α_T as the linear thermal expansion coefficient and T_{ref} an arbitrary reference temperature.

The von Mises criterion, for the time being the most widely used yield criterion for metals, is defined:

$$f = \|\boldsymbol{s}\| - \sqrt{\frac{2}{3}}\,[\sigma_Y + R(\alpha)]\,, \tag{28}$$

with σ_Y denoting the initial yield stress.

Associated to this yield criterion, the following J_2 flow rule is considered:

$$\dot{\boldsymbol{\varepsilon}} = \gamma \boldsymbol{n}, \tag{29}$$

being $\boldsymbol{n} = \boldsymbol{s}/\|\boldsymbol{s}\|$ the normalized stress deviator defining the normal to the Von Mises yield surface $f = 0$ in the deviatoric-stress space, and $\gamma \geq 0$ the consistency parameter. For plastic materials, γ is determined by means of the consistency condition

$$\gamma \dot{f} = 0. \tag{30}$$

Finally, having chosen the equivalent inelastic strain as hardening variable, the flow rule (29) completely defines the hardening law:

$$\dot{\alpha} = \sqrt{\frac{2}{3}}\,\|\dot{\boldsymbol{\varepsilon}}^i\| = \sqrt{\frac{2}{3}}\,\gamma. \tag{31}$$

3.3 Integration of the evolution equations

Following Simo and Taylor,[23] we discretize the evolution laws (29) and (31) using the implicit Euler-backward finite-difference scheme. Then, given the total strain increment $\Delta\boldsymbol{\varepsilon}$ at the particle $\boldsymbol{X}$ during the time interval $[t_n, t_{n+1}]$, $t_{n+1} = t_n + \Delta t$, the material state at $\boldsymbol{X}$ is updated from the previous instant t_n to the current one t_{n+1} by a standard return-mapping algorithm.

Also the consistent tangent matrix was implemented. The correct evaluation of this matrix is essential to achieve good numerical response in the determination of equilibrium condition. In our procedure we have neglected derivatives of stresses with respect to temperature changes without affecting seriously the convergence rate.

3.4 Finite element implementation

Momentum balance equation ignoring inertial effects

$$\nabla \cdot \boldsymbol{\sigma} + \rho \boldsymbol{b} = 0 \quad \forall \boldsymbol{X} \in \Omega_s, \tag{32}$$

subjected to the following boundary conditions

$$\boldsymbol{u} = \bar{\boldsymbol{u}} \quad \forall \boldsymbol{X} \in \partial\Omega_{s,u} \tag{33}$$

$$\boldsymbol{\sigma} \cdot \boldsymbol{n} = \bar{\boldsymbol{t}} \quad \forall \boldsymbol{X} \in \partial\Omega_{s,t}, \tag{34}$$

leads to the standard quasi-static boundary value problem in solid mechanics[24] which consists in finding the displacement field $\boldsymbol{u}$ that satisfy the integral equations

$$\int_{\Omega_s} \boldsymbol{\sigma} : \nabla^s \boldsymbol{w} dV = \int_{\Omega_s} \rho \boldsymbol{b} \cdot \boldsymbol{w} dV + \int_{\partial\Omega_{s,t}} \bar{\boldsymbol{t}} \cdot \boldsymbol{w} dS, \tag{35}$$

throughout the domain Ω_s, for all the admissible displacement weighting functions $\boldsymbol{w}$.

Equation (35) is the weak form of the momentum balance equations (32), where $\rho\boldsymbol{b}$ is the body-force (per unit volume) and $\bar{\boldsymbol{t}}$ is the traction prescribed over the portion $\partial\Omega_{s,t}$ of the boundary (displacement boundary conditions over the complementary portion $\partial\Omega_{s,u}$ are assumed to hold a priori).

Even when linear hexahedral elements are superior to linear tetrahedral elements,[25,26] and they are also better than quadratic tetrahedron elements when plastic deformation occurs,[26] we choose tetrahedron elements for the spatial discretization. This is due to the good availability of procedures for generating arbitrary meshes using tetrahedral elements.

Appropriate mixed finite elements could be employed in order to deal with the numerical difficulties eventually caused by the inelastically-incompressible behavior of metals.[13,24] Although, we have implemented a standard formulation, based in our previous experience in continuous casting simulation.

The displacement trial functions are defined as follows:

$$\boldsymbol{u} = \sum_{i=1}^{n_u} N_i \boldsymbol{U}_i \tag{36}$$

being N_i the displacement shape function associated to the displacement node $i = 1, 2, \ldots, n_u$, $\boldsymbol{U}_i$ the nodal displacement

After replacing $\boldsymbol{u}$ in (35) by its respective finite element approximation (36), and by adopting the corresponding shape functions as weight functions (Galerkin formulation), it yields

$$\boldsymbol{R} = \boldsymbol{F}_{int} - \boldsymbol{F}_{ext} = \boldsymbol{0}, \tag{37}$$

$$\tag{38}$$

where

$$\boldsymbol{F}_{int} = \int_{\Omega_s} \boldsymbol{B}^T \boldsymbol{\sigma}(u)\, \mathrm{d}V \tag{39}$$

$$\boldsymbol{F}_{ext} = \int_{\Omega_s} \boldsymbol{N}^T \rho \boldsymbol{b}\, \mathrm{d}V + \int_{\partial\Omega_{s,t}} \boldsymbol{N}^T \bar{\boldsymbol{t}}\, \mathrm{d}S \tag{40}$$

$\boldsymbol{B}$ is the typical finite element matrix defining the strain-displacement kinematics relation

$$\boldsymbol{\varepsilon} = \boldsymbol{B}\boldsymbol{U}. \tag{41}$$

The nonlinear system of equations (37) is solved iteratively, approximating this system at the i-th iteration using a linear Taylor expansion

$$\boldsymbol{R}_{(\boldsymbol{U}^{(i)})} \approx \boldsymbol{R}_{(\boldsymbol{U}^{(i-1)})} + \boldsymbol{J}_{(\boldsymbol{U}^{(i-1)})} \Delta\boldsymbol{U}^{(i)} = \boldsymbol{0} \tag{42}$$

where $\boldsymbol{J} = \mathrm{d}\boldsymbol{R}/\mathrm{d}\boldsymbol{U}$ is the Jacobian or tangent matrix, and $\Delta\boldsymbol{U}^{(i)} = \boldsymbol{U}^{(i)} - \boldsymbol{U}^{(i-1)}$ is the search direction. Iterative correction of variables is defined by:

$$\Delta\boldsymbol{U}^{(i)} = -[\boldsymbol{J}_{(\boldsymbol{U}^{(i-1)})}]^{-1} \boldsymbol{R}_{(\boldsymbol{U}^{(i-1)})} \tag{43}$$

As described for the thermal problem, this Newton-Raphson scheme is complemented with line-search procedures to accelerate the convergence.

4 THERMO-MECHANICAL COUPLED ANALYSIS

Dependency of the thermal problem on mechanical variables is negligible. Considering this, for every time step the thermal problem is solved first, and then the mechanical problem is solved using as inputs the results of the thermal problem.

Algorithm 1 shows the global calculation scheme. At the time being, a fixed time step is specified. However, more sophisticated schemes, with ability to increment and to reduce the time step will be implemented in the future.

Algorithm 1 Coupled Thermo-Mechanical Analysis

while $t < t_{end}$ **do**
  $t = t + \Delta t$
  $THERMAL\_NEWTON$
  while $\|\boldsymbol{\Psi}_{(\boldsymbol{T}^{(i)})}\| > Tol_{ther}$ **do**
    Calculate $\Delta \boldsymbol{T}^{(i)} = -[\boldsymbol{J}_{(\boldsymbol{T}^{(i-1)})}]^{-1}\boldsymbol{\Psi}_{(\boldsymbol{T}^{(i-1)})}$
    Compute $\boldsymbol{\Psi}_{(\boldsymbol{T}^{(i)})}$
  end while
  $MECHANICAL\_NEWTON$
  while $\|\boldsymbol{R}_{(\boldsymbol{U}^{(i)})}| > Tol_{mech}$ **do**
    Calculate $\Delta \boldsymbol{U}^{(i)} = -[\boldsymbol{J}_{(\boldsymbol{U}^{(i-1)})}]^{-1}\boldsymbol{R}_{(\boldsymbol{U}^{(i-1)})}$
    Compute $\boldsymbol{R}_{(\boldsymbol{U}^{(i)})}$
  end while
end while

5 CONCLUSIONS

We have presented a finite element model to simulate the 3D transient conduction problem with phase-change. The use of linear tetrahedral elements facilitates the exact analytical integration of the finite element arrays, and therefore the exact evaluation of the discrete balance equation. Further, the discontinuous integration procedure let us evaluate correctly the discontinuous nature of phase-change phenomena.

The highly non-linear equation governing the problem is solved using the Newton-Raphson method, with an exact, analytically computed tangent matrix. Such an iterative method provides probably the fastest way to solve this equation. Convergence starting from initial solutions lying out of the "attraction" zone was enforced using a line-search procedure. Therefore, it yields an improvement of the robustness of Newton-Raphson method.

Thermal results were correctly validated against an analytical solution for a non-isothermal phase change problem.

Future work will include more sophisticated time step control and improvements in the mechanical analysis to take into account the incidences of metallurgical transformations on the thermomechanical properties of materials.

REFERENCES

[1] Mackerle J. Finite element analysis and simulation of weldingan addendum: a bibliography (19962001). *Modelling Simul. Mater. Sci. Eng.*, **10**, 295318 (2004).

[2] Tarzia D. A bibliography on moving-free boundary problems for the heat-diffusion equation. the stefan and related problems. *Mat / Serie A : Conferencias, Seminarios Y Trabajos De Matemática No. 2,* (2000).

[3] Porzner H. Possibilities of numerical simulation for evaluation and optimization of welded designs. *ESI Group*.

[4] Nami M., Kadivar M., and Jafarpur K. Three-dimensional thermal response of thick plate weldments: effect of layer-wise and piece-wise welding. *Modelling Simul. Mater. Sci. Eng.*, **12**, 731743 (2004).

[5] Jung G. and Tsai C. Plasticity-based distortion analysis for fillet welded thin-plate t-joints. *Welding Journal*, pages 177–187 (June 2004).

[6] Nigro N., Huespe A., and Fachinotti V. Phasewise numerical integration of finite element method applied to solidification processes. *International Journal of Heat and Mass Transfer*, **43**(7), 1053–1066 (2000).

[7] Fachinotti V. *Modelado Númerico de Fenómenos Termomecánicos en la solidificación y Enfriamiento de Aceros Obtenidos por Colada Continua*. PhD thesis, Universidad Nacional del Litoral-FICH-INTEC, (2001).

[8] Cardona A., Huespe A., and Fachinotti V. Modelado termo-mecánico del proceso de colada continua de aceros. In *Anales del XVIII Congresso Ibero Latino-Amer. de Mét. Comp. para Eng. (XVIII CILAMCE)*, volume I, pages 493–500, Brasília, Brasil, (1997).

[9] Alberg H. and Berglund D. Comparison of an axisymmetric and a three-dimensional model for welding and stress relief heat treatment. Columbus, Ohio, USA, (June 2004). 8th International Conference on Numerical Methods in Industrial Forming Processes, NUMIFORM 2004.

[10] Fachinotti V., Cardona A., and Huespe A. A fast convergent and accurate temperature model for phase-change heat conduction. *Int. J. Numer. Meth. Engng.*, **44** (1999).

[11] Fachinotti V., Cardona A., and Huespe A. Numerical simulation of conduction-advection problems with phase change. *Latin Am. Applied Research, in press*.

[12] Özisik M. and Uzzell J. Exact solution for freezing in cylindrical symmetry with extended freezing temperature range. *Journal of Heat Transfer*, **101**, 331–334 (May 1979).

[13] Zienkiewicz O. and Taylor R. *The Finite Element Method*, volume 1: The Basis. Butterworth-Heinemann, 5th. edition, (2000).

[14] Matthies H. and Strang G. The solution of nonlinear finite element equations. *Int. J. Numer. Meth. Engng.*, **14** (1979).

[15] McDill J., Goldak J., Oddy A., and Bibby M. Isoparametric quadrilaterals and hexahedrons for mesh grading algorithms. *Comm. Appl. Numer. Methods*, **3**, 155–163 (1987).

[16] Tekriwal P. and Mazumder J. Transient and residual thermal strain-stress analysis of gmaw. *ASME J. of Engineering Materials and Technology*, **113**(336-343) (1991).

[17] Lindgren L. Finite element modelling and simulation of welding. part 2: Improved material modelling. *Journal of Thermal Stresses*, **24**(195-231) (2001).

[18] Lemaître J. and Chaboche J. *Mechanics of Solid Materials*. Cambridge University Press, (1994).

[19] Francis J. *Welding Simulations of Aluminum Alloy Joints by Finite Element Analysis*. PhD thesis.

[20] Hughes T. and Belytschko T.(eds.). *Computational Methods for Transient Analysis*.

NORTH-HOLLAND, (1983).

[21] Francis M. and Rahman S. Probabilistic analysis of weld cracks in center-cracked tension specimens. *Computers and Structures*, **76**, 483–506 (2000).

[22] Chang P. and Teng T. Numerical and experimental investigations on the residual stresses of the butt-welded joints. *Computational Materials Science*, **29**(4), 511–522 (2004).

[23] Simo J. and Hughes T. *Computational Inelasticity*. Springer-Verlag, New York, (1998).

[24] Hughes T. *The Finite Element Method. Linear Static and Dynamic Finite Element Analysis*. Prentice-Hall, (1987).

[25] Cifuentes A. and Kalbag A. A performance study of tetrahedral and hexahedral elements in 3-d finite element structural analysis. *Fin. Elem. Anal*, **12**, 313–318 (1992).

[26] Benzley S., Perry E., Merkely K., Clark B., and Sjaardama G. A comparison of all hexagonal and all tetrahedral finite element meshes for elastic and elasto-plastic analysis. *Proc. 14th Ann. Int. Meshing Roundtable, Albuquerque, USA*, (1995).